

# Many-body chiral edge currents and correlated dynamics of atomic spin waves in momentum-space lattices

Yongqiang Li,<sup>1,2</sup> Han Cai,<sup>3</sup> Dawei Wang,<sup>3</sup> Lin Li,<sup>4</sup> Jianmin Yuan,<sup>2</sup> and Weibin Li<sup>5</sup>

<sup>1</sup>*Department of Physics, National University of Defense Technology, Changsha 410073, P. R. China*

<sup>2</sup>*Department of Physics, Graduate School of China Academy of Engineering Physics, Beijing 100193, P. R. China*

<sup>3</sup>*Interdisciplinary Center of Quantum Information and Department of Physics, Zhejiang University, Hangzhou 310027, P. R. China*

<sup>4</sup>*MOE Key Laboratory of Fundamental Physical Quantities Measurement, Hubei Key Laboratory of Gravitation and Quantum Physics, PGMF and School of Physics, Huazhong University of Science and Technology, Wuhan 430074, P. R. China*

<sup>5</sup>*School of Physics and Astronomy, and Centre for the Mathematics and Theoretical Physics of Quantum Non-equilibrium Systems,*

*The University of Nottingham, Nottingham NG7 2RD, United Kingdom*

(Dated: July 21, 2022)

Collective excitations of long-lived atomic hyperfine states can be synthesized into a Bose-Hubbard model in momentum space, where a spatially long-range interaction is introduced by laser-dressing the hyperfine state to Rydberg states. We explore stationary and dynamical properties of the momentum-space lattice in an artificial magnetic field. The many-body ground states support both chiral and anti-chiral edge currents in momentum space. Their stability against strong interactions is verified by a dynamical mean-field simulation. We show that the interplay of the interaction and chirality leads to correlated chiral dynamics, where an interaction-induced excitation blockade in momentum space suppresses the edge currents. When incorporating an effective decay to the lattice, we find that excitation transportation, whose dynamics is governed by a dissipative Bose-Hubbard model, can be prohibited by a strong local dissipation, as a result of the quantum Zeno effect. Our study paves the route to quantum simulate topological phases and exotic dynamics with collective states of interacting atoms in momentum-space lattice.

*Introduction*— Chiral edge states have played an important role in understanding quantum Hall effects [1–3] in solid state materials [4–6]. Ultracold atoms exposed to artificial gauge fields provide an ideal platform to simulate chiral edge currents in and out of equilibrium. This is largely driven by the ability to precisely control and in-situ monitor [7, 8] internal and external degrees of freedom, and atom-atom interactions [9]. Chiral dynamics [10–13] has been examined in the continuum space [14, 15], ladders [16–20], and optical lattices [21–28]. However, chiral states realized in the coordinate space require extremely low temperatures (typical in the order of a few kilo Hz) to protect the topology from being destroyed by motional fluctuations [13]. Up to now, experimental observations of chiral phenomena in ultracold gases are largely at a single-particle level, due to unavoidable dissipations (including spontaneous emission and heating) [9, 29–33], while the realization of many-body chiral edge currents with ultracold atoms is still elusive.

An emerging platform to emulate topological phases is to employ atoms excited to electronically high-lying (Rydberg) states [34–38]. Strong and long-range Rydberg atom interactions (e.g. a few MHz at a distance of several  $\mu\text{m}$  can be reached [39].) allow to investigate dynamics in a short time scale before Rydberg states decay (Rydberg lifetime typically  $10 \sim 100 \mu\text{s}$ ). Furthermore one could use Rydberg dressed states, i.e. electronic ground-states are weakly coupled to Rydberg states, to

achieve longer coherence time [40–45]. Rydberg dressing has been demonstrated experimentally in traps [46], optical tweezers [47] and lattices [48]. This opens opportunities to obtain chiral states of interacting particles by exploiting ultracold atomic gases together with Rydberg interactions.

In this work, we propose a new lattice setup to explore chiral edge currents of an interacting many-body system via hybridizing long-lived hyperfine atomic states with electronically excited Rydberg states. By mapping to momentum space [49], collective excitations (atomic spin waves) of ultracold gases form effective sites of an extended Bose-Hubbard model with competing laser-induced complex hopping and on-site Rydberg interactions. With this new setup, previously untouched many-body phases and correlated chiral dynamics can be realized in momentum-space lattice (MSL). Through dynamical mean-field calculations, we identify novel chiral edge currents in the many-body ground state. We show that the strong on-site interaction alters dynamics of chiral edge currents qualitatively. By incorporating decay to the system, we find a regime where transportation of the collective excitation in momentum space is largely coherent in the dissipative limit, rooted from the quantum Zeno effect.

*The model*— Collective atomic excitations stored in long-lived hyperfine states  $|a\rangle$  and  $|b\rangle$  [Fig. 1(a)] are created by an off-resonant and a resonant standing wave lasers with wave vector  $\mathbf{k}$  (wave length  $\lambda = 2\pi/|\mathbf{k}|$ ).

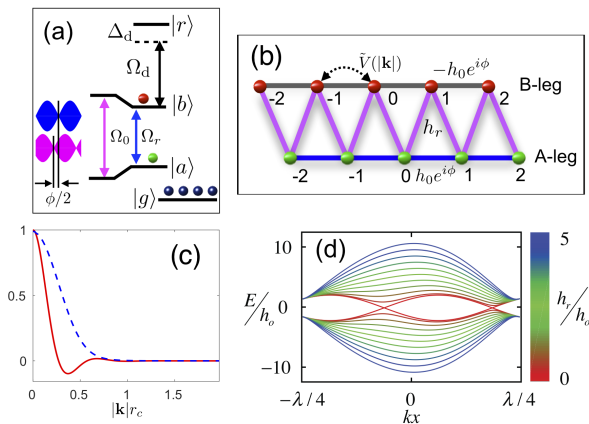


FIG. 1. (Color online) **Interacting spin waves in momentum-space lattices.** (a) Level scheme. Collective excitations in states  $|a\rangle$  and  $|b\rangle$  are coupled resonantly by a detuned (magenta, Rabi frequency  $\Omega_0$ ) and a resonant (blue, Rabi frequency  $\Omega_r$ ) standing wave laser, forming a momentum-space lattice. When weakly coupled to a Rydberg state, atoms in state  $|b\rangle$  experience an effective interaction  $V(|\mathbf{R}|)$ . (b) Two-leg zig-zag lattice. The state  $|a\rangle$  ( $|b\rangle$ ) sits on the A-leg (B-leg) of the ladder. Hopping rate along the A-leg (B-leg) is  $h_o e^{i\phi}$  ( $-h_o e^{i\phi}$ ). The interleg hopping is determined by parameter  $h_r$ . The interactions between sites in the B-leg is determined by  $\tilde{V}(|\mathbf{k}|)$ . (c) Momentum dependent interaction  $\tilde{V}(|\mathbf{k}|)/\tilde{V}(0)$  (solid) and collective decay  $\Gamma_k/\Gamma_0$  (dashed). The latter is relevant only when a superradiance lattice is considered [49]. Using parameters  $\lambda = 785$  nm and  $r_c = 4.5$   $\mu\text{m}$ , the resulting interaction is only important when  $k \leq k_c = 2\pi/\lambda$ . (d) Band structure of the noninteracting ladder as a function of real-space coordinate  $x$  for different hopping amplitudes and flux  $\phi = \pi/4$ .

For small number of excitations, the atomic spin waves are described by free bosons [49]. We focus on a one-dimension case when the standing wave lasers are along the same direction. By projecting the spin wave to momentum space with a characteristic momentum  $k_c$  [49], we obtain a ladder of A-leg and B-leg for the  $|a\rangle$  and  $|b\rangle$  states [Fig. 1(b)], respectively. The  $j$ -th site of A-leg (B-leg) represents a collective state with wave vector  $2jk_c$  [ $(2j-1)k_c$ ]. When the standing wave lasers are phase mismatched [Fig. 1(a)], a synthetic magnetic field is generated [50], which leads to an induced nearest-neighbor hopping with complex amplitudes along and between the ladders. In addition, state  $|b\rangle$  couples to a Rydberg state by an off-resonant laser, resulting in a Rydberg dressed interaction  $V(|\mathbf{r}|) \equiv C/(r_c^6 + |\mathbf{r}|^6)$ , where  $C$  and  $r_c$  are the dispersion coefficient and characteristic distance of the soft-core shape interaction, respectively [42–45]. Hamiltonian of the ladder is given by an extended Bose-Hubbard model,

$$H = \sum_i \left[ -h_r (b_{i-1}^\dagger a_i + a_i^\dagger b_i) - h_o e^{i\phi} (a_i^\dagger a_{i+1} - b_i^\dagger b_{i+1}) + \text{H.c.} \right] + \sum_{p,i,l} \tilde{V}(p) b_{i+p}^\dagger b_i b_{l-p}^\dagger b_l - \sum_{i,\sigma=a,b} \mu_{i\sigma} n_{i\sigma} \quad (1)$$

where  $n_i^{(\sigma)} = \sigma_i^\dagger \sigma_i$  is the atomic density in state  $|\sigma\rangle$  ( $\sigma = a, b$ ) at site (momentum)  $i$ .  $h_o$  and  $h_r$  are the hopping amplitudes.  $\phi$  and  $\mu_\sigma$  are the flux and chemical potential.  $\tilde{V}(k) = \sum_{\mathbf{r}} \exp^{-i\pi k \cdot \mathbf{R}} V(|\mathbf{r}|)$  is the Fourier transformation of the interaction potential  $V(|\mathbf{r}|)$ . The interaction  $\tilde{V}(k)$  is short-ranged (on-site) in momentum space as typically  $r_c \gg \lambda$  [Fig. 1(c)]. Details of the Hamiltonian can be found in the Supplemental Material (SM).

*Chiral edge currents and ground-state phase diagram*—When the two-body interaction vanishes ( $\tilde{V}(k) = 0$ ), Hamiltonian (1) possesses  $[\tau H(\phi)\tau^{-1} = H(-\phi)]$ ,  $[\mathcal{C}H(\phi)\mathcal{C}^{-1} = H(\pi + \phi)]$ , and  $[\mathcal{T}H(\phi)\mathcal{T}^{-1} = H(2\pi + \phi)]$ , where  $\tau$ ,  $\mathcal{C}$  and  $\mathcal{T}$  are the time-reversal, chiral and translational symmetry operators. The chiral symmetry shows that currents after swapping the two states will remain the same if the flux is shifted simultaneously by  $\pi$ , i.e.  $\phi \rightarrow \phi + \pi$ . The system does not preserve the time-reversal symmetry in general except  $\phi = \pi/2$ , where the ground state energy exhibits double degeneracy [50], leading to rich chiral phases (see Fig. S1 in SM for examples).

We first solve the Hamiltonian exactly by excluding the two-body interaction, obtaining three types of band minima, i.e. a single minimum at real-space coordinate  $x = 0$  or  $\neq 0$ , and two minima, as show in Fig. 1(d). Correspondingly, three distinctive chiral phases are expected. These phases are characterized by current  $J_{\sigma\sigma'} \equiv -2\text{Im}(h_{i,j}\langle\sigma_i^\dagger\sigma_j'\rangle)$  for the bond  $j \rightarrow i$  and the leg  $\sigma \rightarrow \sigma'$ , similar to the definition in real-space lattices [51, 52]. As shown in Fig. 2, the ground state prefers a number of chiral superfluid phases (CSFs). When the inter-leg coupling  $h_r$  is strong, currents along the ladders (edges) have opposite directions, i.e.  $J_{AA} \times J_{BB} < 0$  and  $J_{AB} = 0$  [Fig. 2(c)], denoted by CSF<sub>m</sub> phase (condensed into band minimum at  $x = 0$ ). When both  $h_r$  and  $h_o$  are comparable, we have a different chiral superfluid phase (CSF<sub>v</sub> condensed into band minimum at  $x \neq 0$ ) where currents on the ladders and rungs satisfy  $J_{AA} \times J_{BB} < 0$ , and  $J_{AB} \neq 0$ . The CSF<sub>m</sub> and CSF<sub>v</sub> phases are analogues of the Meissner and vortex phases of real-space ladder systems [16–19, 53–61]. When  $h_r$  is further decreased, a new quantum phase (CSF<sub>p</sub> condensed into two degenerate band minima) emerges in momentum-space lattice, where currents on both ladders flow in the same direction (anti-chiral edge current), i.e.  $J_{AA} \times J_{BB} > 0$ , similar to the ground-state persistent current in normal metal rings threading an external magnetic flux [62–66]. The presence of the anti-chiral edge current is a result of the superposition of the doubly degenerate ground states (Details of the condensation distribution and currents of the CSF<sub>p</sub> phase are shown in SM).

The CSF<sub>s</sub> phases are stable against atomic interactions and survive in a large parameter regime. This is verified by a bosonic dynamical mean-field calculation that captures both quantum fluctuations and strong correlations in a unified framework [51, 52, 68], as shown

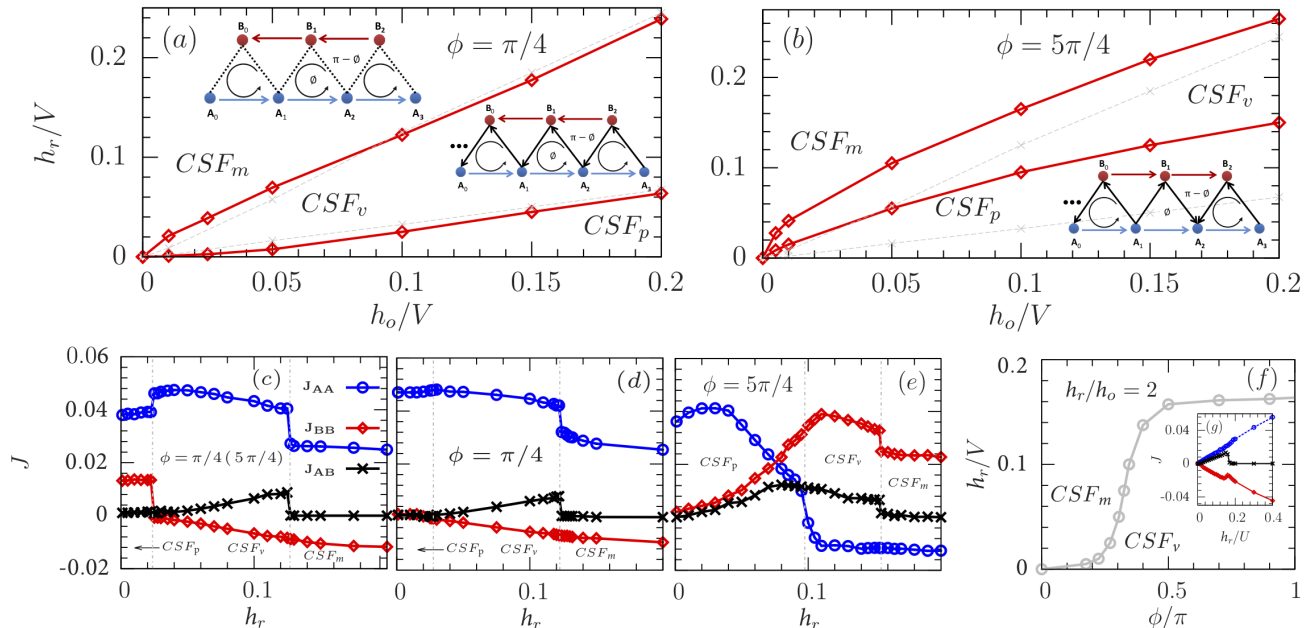


FIG. 2. (Color online) **Strongly correlated many-body ground states.** (a)(b) Interaction effects on phase diagrams in momentum-space lattice in terms of hopping amplitude  $h_r$  and  $h_o$  for different flux. There are three quantum phases with different types of edge currents, including the  $CSF_m$  and  $CSF_v$  phases with chiral edge currents, and the  $CSF_p$  phase with anti-chiral edge current. Here, the filling  $N_{\text{tot}}/N_{\text{lat}} = 0.125$  with  $N_{\text{tot}}$  being the total number of atoms in the lattice and  $N_{\text{lat}}$  the lattice size [67], and the dashed lines denote the non-interacting system. Interaction effects on phase transitions for a non-interacting (c) and interacting (d)(e) systems. Note that in the absence of two-body interactions, the currents for  $\phi = 5\pi/4$  can be obtained from (c) by using the chiral symmetry (i.e. swapping the state  $|a\rangle$  and  $|b\rangle$ ). The other parameters  $h_o = 0.1$  and  $V = 0$  (c);  $h_o = 0.1$  and  $V = 1$  (d);  $h_o = 0.1$  and  $V = 1$  (e). (f) Interplay between flux and interaction for a fixed hopping amplitude ratio. Inset: Interaction-induced  $CSF_v$ - $CSF_m$  phase transition for a fixed flux  $\phi = 0.6\pi$  (g). Periodic boundary condition is used in the calculation.

in Fig. 2(a)(b). The reliability of this approach (see SM for details) has been confirmed by a comparison with an unbiased quantum Monte Carlo simulation [69]. A direct consequence of the two-body interaction is that it breaks the chiral symmetry [ $\mathcal{C}H(\phi)\mathcal{C}^{-1} = H(\pi + \phi)$ ]. This is especially visible in the  $CSF_p$  phase, where the phase region shrinks for  $\phi = \pi/4$  [Fig. 2(a)] but expands for  $\phi = 5\pi/4$  [Fig. 2(b)]. One might expect the B-leg current  $J_{BB}$  is suppressed in the strongly interacting regime. Instead, the two-body interactions reduce the energy separation between the two legs when  $\phi = 5\pi/4$ , and the interplay of the hopping and interaction increases the currents  $J_{BB}$  and  $J_{AB}$  in the intermediate hopping regime. In the weakly interacting regime, the currents coincide with the noninteracting case, as shown in Fig. 2(c)-(e). Besides changing the hopping, one can moreover drive transitions between the  $CSF_s$  phases by varying the flux  $\phi$ . In Fig. 2(f), we show that the Meissner phase is driven to the vortex phase by changing the flux.

*Excitation blockade, chiral and Zeno dynamics*— The controllability of the parameters and initial states permits to study correlated chiral dynamics in MSL. This is illustrated by a situation where initially two excitations at the first site of A-leg (i.e.  $n_1^{(a)} = 2$ ) are prepared (see

SM for details). When the atomic interaction is negligible, a large fraction of the excitation can be transferred to the B-leg, as shown in Fig. 3(a). Turning on the interaction, the excitation probability in the B-leg is reduced. A closer examination shows that the double occupation probability  $P_2 = \sum_j |\langle \psi(t) | (b_j^\dagger)^2 / \sqrt{2} | 0 \rangle|^2$  at given sites in the B-leg is significantly suppressed, due to the strong on-site interaction, where  $|\psi(t)\rangle = \exp(-iHt)|\psi(t=0)\rangle$  is the many-body state at time  $t$ . This excitation suppression could be regarded as an interaction blockade in momentum space, analogue to the Rydberg blockade effect in real space [70, 71].

Dynamical evolution of currents is altered by the two-body interaction as well. Due to the strong interaction, the intensity of the currents becomes smaller in general. Interestingly, we find that the currents exhibit certain features of the ground-state phases of the Eq. (1). When the parameters are in the  $CSF_v$  phase, for example, the currents counter-propagate on the two legs at the beginning of the evolution [Fig. 3(c)-(e)]. Surprisingly, the currents for  $\phi = 5\pi/4$  along the legs become co-propagating when two-body interactions are important [Fig. 3(f)]. This behavior is similar to the currents found in the  $CSF_p$  phase.

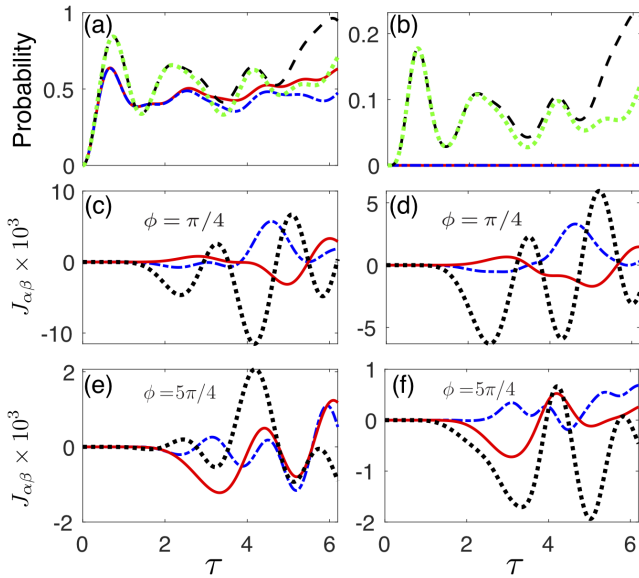


FIG. 3. (Color online) **Dynamics of excitations and currents.** (a) Total excitation and (b) double occupation probability of the B-leg. Dotted and dashed curves correspond to non-interacting situations and dot-dashed and solid with two-body interactions. The flux is  $\phi = \pi/4$  (solid and dashed) and  $\phi = 5\pi/4$  (dot-dashed and dotted). Time evolution of currents in the absence (c)(e) and presence (d)(f) of two-body interactions, with currents along the A-leg  $J_{AA}$  (dotted), B-leg  $J_{BB}$  (solid), and between the two legs  $J_{AB}$  (dashed). Other parameters are  $h_o = h_r = 0.02$  and  $V = 0$  (c)(e), and  $h_o/V = h_r/V = 0.02$  (d)(f). We have defined  $\tau \equiv h_o t$ .

In the remaining part of this work, we turn to a different regime where an effective decay of the spin wave is introduced (or one replaces the spin wave state with the so-called timed Dicke state to implement a superradiance lattice [49]). To highlight the collective decay, we study dissipative dynamics of the A-leg solely. As two-body interactions are absent, we will study a single excitation in the A-leg, whose dynamics is now described by a master equation

$$\dot{\rho} = -i[H, \rho] + \sum_j \Gamma_j (a_j \rho a_j^\dagger - \{a_j^\dagger a_j, \rho\}), \quad (2)$$

where  $\Gamma_j$  are decay rate of the  $j$ -th site. Propagation of the spin wave depends on hopping  $h_o$  and decay rate  $\Gamma_j$ . The latter is site (momentum) dependent for a superradiance lattice. With this consideration,  $\Gamma_j \neq 0$  only for phase matched spin wave components [72], i.e. at sites with index  $j = 0$  and 1 [see Fig. 1(b)].

We consider a single excitation initially occupies the state  $|n_{-4}^{(a)} = 1\rangle$  and propagates to the middle of the lattice. One typically expects that the propagation is coherent away from the central sites, and becomes dissipative once approaching to the decaying sites. This is true when the decay rate  $\Gamma_j$  is small, where a large fraction of the population will be lost [Fig. 4(a)]. The dynamics changes

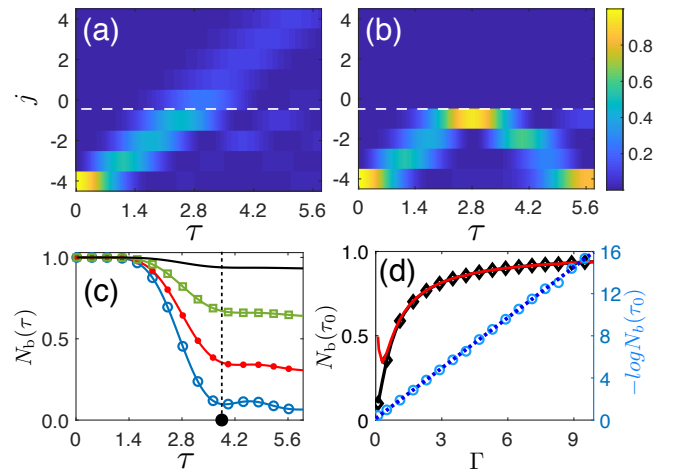


FIG. 4. (Color online) **Zeno dynamics in the dissipative regime.** Loss (a) and reflection (b) of the spin wave. Without decay of the spin wave, population propagates along the lattice and losses at the zeroth and first sites. Strong dissipation in site  $|n_0^{(a)}\rangle$  and  $|n_1^{(b)}\rangle$  reflects the population. In (a)  $\Gamma_0 = \Gamma_1 = \Gamma = 0.01$  and (b)  $\Gamma_0 = \Gamma_1 = \Gamma = 2.0$ , while decay in other sites being negligible. (c) The remaining population  $N_b(\tau)$  (from the initial site to the middle of the lattice, denoted by the dashed line.) is show at different times for decay rate  $\Gamma_0 = \Gamma_1 = \Gamma$  from 0.1 (circle), 0.5 (star), and 1.5 (square) to 10 (solid). (d) Saturation values (diamond) of the remaining population at  $\tau = h_o t = 3.8$ . When the decay is strong, the total population (red solid) is identical the reflected population, i.e. fully reflected. The remaining population depends on  $\Gamma$  exponentially (circles). The dashed line is the fitting of  $-\log N_b(\tau_0)$ . Other parameters are  $\phi = 0$ ,  $h_o = h_r = 0.2$ .

qualitatively when  $\Gamma_j$  is large, where the population is largely reflected at the zeroth site [Fig. 4(b)(c)].

We attribute the reflection to the quantum Zeno effect [73]. Stronger decay behaves similar to a frequent measurement of occupations in the zeroth site. It prohibits the occupation of its neighboring sites from hopping to the initially not occupied center sites. As a result, the loss occurs at an effective, smaller rate  $h_o/\Gamma_0^2$  [74] (see SM for details). To verify this, we numerically calculate the remaining population as a function of  $\Gamma_0$  at time  $\tau = h_o t = 3.8$ , when the reflection occurs. As shown in Fig. 4(d), the effective decay rate is linearly proportional to  $\sim h_o/\Gamma_0^2$ , confirming the analytical prediction.

*Conclusion*— A momentum-space lattice model suitable for studying topological physics and correlated many-body dynamics is proposed. Compared to schemes based on superradiant Dicke states characterized by steady states in momentum space [49, 50, 75], our setting opens opportunities to explore correlated chiral phenomena both in and out of equilibrium coherently. The zero-temperature ground states exhibit broken chiral symmetry, signified by a number of chiral quantum phases that are stabilized against the two-body interaction. Dynamics of the population and current between the two lad-

ders is suppressed by the two-body interaction, leading to a blockade in momentum space. We show that quantum Zeno effect can be studied in the presence of a site-dependent dissipation. A comprehensive experimental implementation of the setting is provided.

Our study paves new routes towards the study of chirality with interacting spin waves in higher dimensions and with external driving. In higher dimensional frustrated lattices, such as honeycomb lattice, emergent topology of quantum dynamics can be investigated in a coherent system, e.g., by quenching the system from a trivial state to topological regimes. Another interesting question here is whether topological signatures can be uncovered in an open quantum system to understand the stability of edge modes against dissipative channels. This can be extended to explore, e.g., many-body dynamical phase transitions as a result of the interplay between the strong atomic interaction and dissipation.

### ACKNOWLEDGEMENTS

We would like to thank helpful discussions with Jing Zhang, Yinghai Wu, Xiongjun Liu and Tao Shi. This work is supported by the National Natural Science Foundation of China under Grants No. 11304386 and No. 11774428 (Y. L.). D. W. acknowledges support from the National Natural Science Foundation of China (No. 11874322) and the National Key Research and Development Program of China (Grants No. 2018YFA0307200). W. L. acknowledges support from the UKIERI-UGC Thematic Partnership No. IND/CONT/G/16-17/73, EPSRC Grant No. EP/M014266/1 and EP/R04340X/1. The numerical calculations were carried out at National Supercomputer Center in Tianjin, and on TianHe-1A.

# Supplementary Material

## EXTENDED BOSE-HUBBARD MODEL IN MOMENTUM SPACE

### The Hamiltonian in momentum space

Here we consider  $N$  three-level atoms, i.e. ground state  $g(\mathbf{r}_i)$ , another ground state  $a(\mathbf{r}_i)$  and Rydberg dressed state  $b(\mathbf{r}_i)$ , where  $\mathbf{r}_i$  is the position of the  $i$ th atom with random distribution. The atoms are initially prepared in the ground state  $|G\rangle \equiv |g_1 \dots g_N\rangle$ . A standing wave laser couples the atomic  $a$  and  $b$  states with vectors  $\mathbf{k}_1 = -\mathbf{k}_2 = \mathbf{k}_c$ . In the rotating wave approximation, the Hamiltonian reads

$$H = \left(-\sum_j h_r (e^{i\mathbf{k}_1 \cdot \mathbf{r}} + e^{i\mathbf{k}_2 \cdot \mathbf{r}}) |b_j\rangle \langle a_j| + \text{H.c.}\right) + \sum_{i \neq j}^N \frac{C}{r_c^6 + |\mathbf{r}|^6} |\dots b_i \dots b_j \dots\rangle \langle \dots b_i \dots b_j \dots|, \quad (\text{S1})$$

where  $C$  and  $r_c$  is the dispersion coefficient and characteristic distance of the soft-core shape interaction, respectively [S42–S45]. Collective atomic excitation operators in momentum space are introduced as

$$a_l^\dagger \equiv \frac{1}{\sqrt{N}} \sum_{i=1}^N e^{i2lk_c r_i} |\dots a_i \dots\rangle \langle G|, \quad (\text{S2})$$

$$b_l^\dagger \equiv \frac{1}{\sqrt{N}} \sum_{i=1}^N e^{i(2l-1)k_c r_i} |\dots b_i \dots\rangle \langle G|, \quad (\text{S3})$$

We transform the Hamiltonian from position space to momentum space via

$$|\dots a_i \dots\rangle \langle G| \equiv \frac{1}{\sqrt{N}} \sum_l e^{-i2lk_c r_i} a_l^\dagger, \quad (\text{S4})$$

$$|\dots b_i \dots\rangle \langle G| \equiv \frac{1}{\sqrt{N}} \sum_l e^{-i(2l-1)k_c r_i} b_l^\dagger. \quad (\text{S5})$$

The total Hamiltonian in momentum space can be written as

$$H = -\sum_i h_r (b_{i-1}^\dagger a_i + a_i^\dagger b_i) + \text{H.c.} \\ + \sum_{i_1, i_2, i_3, i_4} \tilde{V}(\Delta i) b_{i_1}^\dagger b_{i_2} b_{i_3}^\dagger b_{i_4} \delta_{i_1 - i_2 + i_3 - i_4}, \quad (\text{S6})$$

where  $\tilde{V}(\Delta i) \equiv \tilde{V}(i_1 - i_2) = \sum_R e^{-\pi i(i_1 - i_2)k \cdot R} V(R)$ , and the transformation is valid for many excitations if the excitation number is much less than the atom number [S49].

Here, if we switch on another far-tuned standing wave lasers, then an extra interaction term  $-\sum_j 2h_o \cos(2k_c r_j + \phi) (|a_j\rangle \langle a_j| - |b_j\rangle \langle b_j|)$  appears due to the AC Stark shifts [S50]. The total Hamiltonian is given by:

$$H = -\sum_i h_r (b_{i-1}^\dagger a_i + a_i^\dagger b_i) + \text{H.c.} \\ -\sum_i e^{i\phi} h_o (a_i^\dagger a_{i+1} - b_i^\dagger b_{i+1}) + \text{H.c.} \\ + \sum_{p, i, l} \tilde{V}(p) b_{i+p}^\dagger b_i b_{i-p}^\dagger b_l. \quad (\text{S7})$$

## BOSONIC DYNAMICAL MEAN-FIELD THEORY

To investigate ground states of bosonic gases loaded into momentum-space lattices, described by Eq. (1), we establish a bosonic version of dynamical mean-field theory (BDMFT) on the ladder system with  $z = 4$ , where  $z$  is the number of neighbors connected by hopping terms. As in fermionic dynamical mean field theory, the main idea of the BDMFT approach is to map the quantum lattice problem with many degrees of freedom onto a single site - "impurity site" - coupled self-consistently to a noninteracting bath [S76]. The dynamics at the impurity site can thus be thought of as the interaction (hybridization) of this site with the bath. Note here that this method is exact for infinite dimensions, and is a reasonable approximation for neighbors  $z \geq 4$ . In the noninteracting limit, the problem is trivially solvable in all dimensions, all correlation functions factorize and the method becomes exactly [S77].

### BDMFT equations

In deriving the effective action, we consider the limit of a high but finite dimensional optical lattice, and use the cavity method [S76] to derive self-consistency equations within BDMFT. In the following, we use the notation  $h_{ij}$  for the hopping amplitude between sites  $i$  and  $j$ , and define creation field operator  $b^\dagger$  for the state  $|\sigma\rangle$  [ $\sigma = a(b)$ ] to shorten Ham. (1). And then the effective action of the impurity site up to subleading order in  $1/z$  is then expressed in the standard way [S76, S77], which is described by:

$$S_{\text{imp}}^{(0)} = - \int_0^\beta d\tau d\tau' \sum_{\sigma\sigma'} \begin{pmatrix} b^{(0)*}(\tau) & b^{(0)}(\tau) \end{pmatrix} \mathcal{G}^{(0)-1}(\tau - \tau') \begin{pmatrix} b^{(0)}(\tau') \\ b^{(0)*}(\tau') \end{pmatrix} \quad (\text{S8})$$

$$+ \int_0^\beta d\tau \sum_{j,p} V b^{(i+p)*}(\tau) b^{(i)}(\tau) b^{(j-p)*}(\tau) b^{(j)}(\tau),$$

with Weiss Green's function

$$\mathcal{G}^{(0)-1}(\tau - \tau') \equiv - \quad (\text{S9})$$

$$\begin{pmatrix} (\partial_{\tau'} - \mu)\delta + \sum_{\langle 0i \rangle, \langle 0j \rangle} h_{ij}^2 G_{ij}^1(\tau, \tau') & \sum_{\langle 0i \rangle, \langle 0j \rangle} h_{ij}^2 G_{ij}^2(\tau, \tau') \\ \sum_{\langle 0i \rangle, \langle 0j \rangle} h_{ij}^2 G_{ij}^{2*}(\tau', \tau) & (-\partial_{\tau'} - \mu_\sigma)\delta + \sum_{\langle 0i \rangle, \langle 0j \rangle} h_{ij}^2 G_{ij}^1(\tau', \tau) \end{pmatrix},$$

and superfluid order parameter

$$\Phi_i(\tau) \equiv \langle b_i(\tau) \rangle_0. \quad (\text{S10})$$

Here, we have defined the the diagonal and off-diagonal parts of the connected Green's functions

$$G_{ij}^1(\tau, \tau') \equiv -\langle b_i(\tau) b_j^*(\tau') \rangle_0 + \Phi_i(\tau) \Phi_j^*(\tau'), \quad (\text{S11})$$

$$G_{ij}^2(\tau, \tau') \equiv -\langle b_i(\tau) b_j(\tau') \rangle_0 + \Phi_i(\tau) \Phi_j(\tau'), \quad (\text{S12})$$

where  $\langle \dots \rangle_0$  denotes the expectation value in the cavity system (without the impurity site).

To find a solver for the effective action, we return back to the Hamiltonian representation and find that the local Hamiltonian is given by a bosonic Anderson impurity model

$$\hat{H}_A^{(0)} = - \sum t \left( \Phi^{(0)*} \hat{b}^{(0)} + \text{H.c.} \right) + V \sum_{i,j,p} b_{j+p}^\dagger b_j b_{i-p}^\dagger b_i + \sum_l \epsilon_l \hat{a}_l^\dagger \hat{a}_l + \sum_l \left( V_l \hat{a}_l \hat{b}^{\dagger(0)} + W_{\sigma,l} \hat{a}_l \hat{b}^{(0)} + \text{H.c.} \right), \quad (\text{S13})$$

where the chemical potential and interaction term are directly inherited from the Hubbard Hamiltonian. The bath of condensed bosons is represented by the Gutzwiller term with superfluid order parameters  $\Phi^{(0)}$ . The bath of normal bosons is described by a finite number of orbitals with creation operators  $\hat{a}_l^\dagger$  and energies  $\epsilon_l$ , where these orbitals are coupled to the impurity via normal-hopping amplitudes  $V_l$  and anomalous-hopping amplitudes  $W_l$ . The anomalous hopping terms are needed to generate the off-diagonal elements of the hybridization function.

The Anderson Hamiltonian can be implemented in the Fock basis, and the corresponding solution can be obtained by exact diagonalization of BDMFT [S76]. After diagonalization, the local Green's function, which includes all the

information about the bath, can be obtained from the eigenstates and eigenenergies in the Lehmann-representation

$$G_{\text{imp}}^1(i\omega_n) = \frac{1}{Z} \sum_{mn} \langle m|\hat{b}|n\rangle \langle n|\hat{b}^\dagger|m\rangle \frac{e^{-\beta E_n} - e^{-\beta E_m}}{E_n - E_m + i\hbar} + \beta\Phi\Phi^* \quad (\text{S14})$$

$$G_{\text{imp}}^2(i\omega_n) = \frac{1}{Z} \sum_{mn} \langle m|\hat{b}|n\rangle \langle n|\hat{b}|m\rangle \frac{e^{-\beta E_n} - e^{-\beta E_m}}{E_n - E_m + i\hbar\omega_n} + \beta\Phi\Phi. \quad (\text{S15})$$

Integrating out the orbitals leads to the same effective action as in Eq. (S8), if the following identification is made

$$\Delta(i\omega_n) \equiv t^2 \sum'_{\langle 0i\rangle, \langle 0j\rangle} \mathbf{G}_{ij}^{(0)}(i\omega_n), \quad (\text{S16})$$

where  $\Delta^1(i\omega_n) \equiv -\sum_l \left( \frac{V_l V_l^*}{\epsilon_l - i\omega_n} + \frac{W_l^* W_l}{\epsilon_l + i\omega_n} \right)$ ,  $\Delta^2(i\omega_n) \equiv -\sum_l \left( \frac{V_l W_l^*}{\epsilon_l - i\omega_n} + \frac{W_l^* V_l}{\epsilon_l + i\omega_n} \right)$ , and  $\sum'$  means summation only over the nearest neighbors of the "impurity site".

In next step, we make the approximation that the lattice self-energy  $\Sigma_{i,\text{lat}}$  coincides with the impurity self-energy  $\Sigma_{i,\text{imp}}$ , which is obtained from the local Dyson equation

$$\Sigma_{i,\text{imp}}(i\omega_n) = \begin{pmatrix} i\omega_n + \mu + \Delta^1 & \Delta^2 \\ \Delta^{2*} & -i\omega_n + \mu + \Delta^{1*} \end{pmatrix} - G_{ii,\text{imp}}^{-1}(i\omega_n). \quad (\text{S17})$$

The real-space Dyson equation takes the following form:

$$G_{ij,\text{latt}}^{-1}(i\omega_n) = \begin{pmatrix} (i\omega_n + \mu - \Sigma_{i,\text{lat}}^{11}) \delta_{ij} + h_{ij} & -\Sigma_{i,\text{lat}}^{12} \delta_{ij} \\ -\Sigma_{i,\text{lat}}^{21} \delta_{ij} & (-i\omega_n + \mu - \Sigma_{i,\text{lat}}^{22}) \delta_{ij} + h_{ij} \end{pmatrix}. \quad (\text{S18})$$

Here, the self-consistency loop is closed by Eq. (S14)-(S18), and this self-consistency loop is repeated until the desired accuracy for values of parameters  $\epsilon_l$ ,  $V_l$  and  $W_l$  and superfluid order parameter  $\Phi$  is obtained.

### GROUND-STATE PHASE DIAGRAM FOR $\phi = \pi/2$

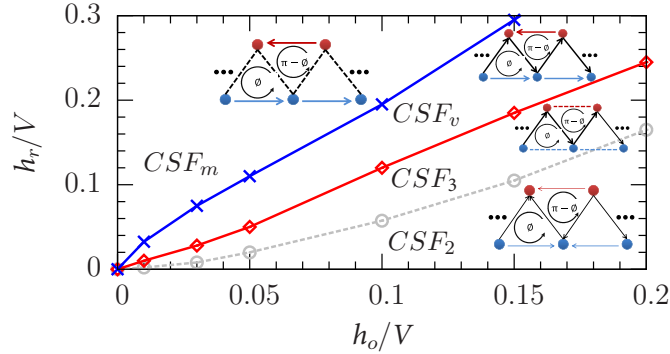


FIG. S1. (Color online) Phase diagram of the quantum system with interacting spin wave states in a momentum-space lattice with the flux  $\phi = \pi/2$  and filling factor  $N_{\text{tot}}/N_{\text{lat}} = 0.125$ .

Actually, there are two special case for the flux  $\phi = 0$  and  $\phi = \pi/2$ . For the case  $\phi = 0$ , the phenomena are trivial, and the system does not support edge currents in the absence (presence) of Rydberg long-range interactions. For the case  $\phi = \pi/2$ , the band structure of the lattice system is actually a double-valley well with two degenerate band minima connected by time-reversal symmetry, indicating that more ground states appear in the case. Here we choose the parameters: the filling factor  $N_{\text{tot}}/N_{\text{lat}} = 0.125$  ( $N_{\text{lat}}$  being the lattice size) and  $\phi = \pi/2$ . We observe there are four stable phases in the diagram with different types of ground-state edge currents, including  $\text{CSF}_m$  with currents only on the ladders, and  $\text{CSF}_v$  with currents on both ladders and rungs. The physical reason of the suppressed edge currents of the  $\text{CSF}_2$  and  $\text{CSF}_3$  phases is that,  $J_{AA}^i \approx 2h_o n_i \sin(\phi - 2kx_A) \approx 0$  and  $J_{BB}^i \approx -2h_o n_i \sin(\phi - 2kx_B) \approx 0$  with  $\phi = \pi/2$ ,  $n_i$  being the filling at site  $i$ , and condensing at  $2kx_A \approx \pi/2$  and  $2kx_B \approx -\pi/2$ , respectively.



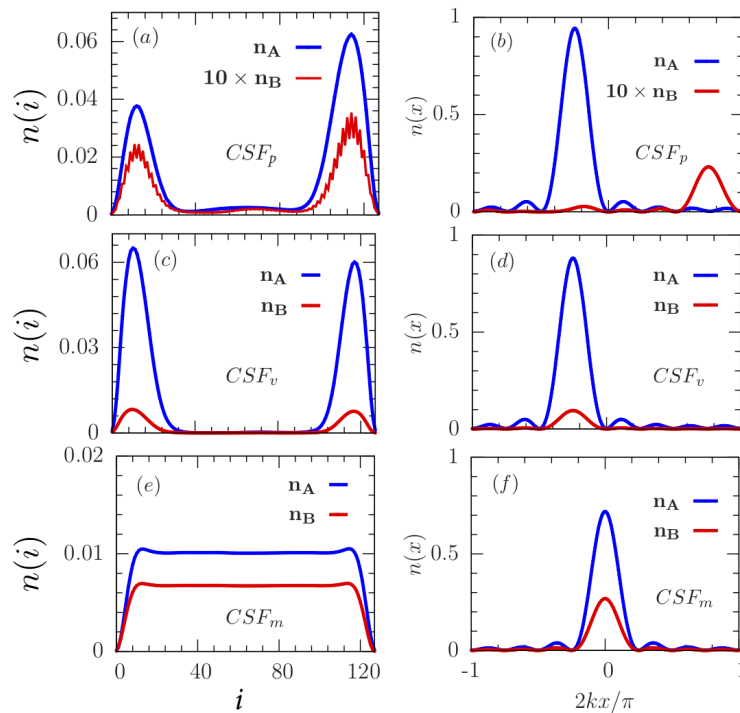


FIG. S2. (Color online) **Ground-state density distribution of interacting spin waves with open boundary condition.** The momentum-space density distributions are shown for the  $CSF_p$  (a),  $CSF_v$  (c) and  $CSF_m$  (e) phases. The corresponding real-space density distributions are shown in (b), (d) and (f). Here the flux is  $\phi = \pi/4$ , the parameters  $h_r/V$  and  $h_o/V$  are 0.005 and 0.2 in the  $CSF_p$  phase, 0.1 and 0.2 in the  $CSF_v$  phase, and 0.3 and 0.2 in the  $CSF_m$  phase, respectively.

## DENSITY DISTRIBUTION IN REAL SPACE AND MOMENTUM SPACE

The density distributions in momentum and real space are vastly different in the three phases. Here we will show both real-space and momentum-space density distributions in these phases, which might be observed directly through time-of-flight experiment. In the Meissner phase, the size of the vortex is infinite and the density is uniform in the momentum-space lattice. On the other hand, in the  $CSF_p$  and  $CSF_v$  phases, the system exhibits vortex structures, where the densities are distributed inhomogeneously and the vortexes are separated into different regions (the averaged inter-leg current  $\sum_i J_{BB}^i/N_{\text{lat}} \approx 0$  and  $\neq 0$  for the  $CSF_p$  and  $CSF_v$  phases, respectively).

Actually, we have observed that there are three different kinds of band structures in the noninteracting system, as shown in Fig. 1(d), where band minima are localized at zero ( $CSF_m$ ), finite-value ( $CSF_v$ ), and doubly degenerate points ( $CSF_p$ ) in real space [S50]. The interacting system also supports three types of condensation in real space, and the resulting phenomena are that, in the  $CSF_p$  phase, the maximal density of the  $|a\rangle$  and  $|b\rangle$  states separates by about  $2kx \approx \pi$ , and in the  $CSF_v$  phase, peak positions of the two states are identical in real space condensing at nonzero value. In the  $CSF_m$  phase, however, the maximal value of the density in the two states is centered at  $2kx = 0$  in real space. This indicates that we can directly identify the  $CSF_p$  phase through the real-space distribution.

## $CSF_p$ PHASE WITHOUT TWO-BODY INTERACTIONS

When the two-body interaction is vanishing, the Hamiltonian of an ensemble of atoms in real space is given by

$$H = \sum_j 2h_0 \cos(2kx_j - \phi)(|b_j\rangle\langle b_j| - |a_j\rangle\langle a_j|) - 2h_r(|a_j\rangle\langle b_j + |b_j\rangle\langle a_j|), \quad (\text{S19})$$

where  $j$  is the index of atoms. The eigenvalues of the Hamiltonian are  $E_{\pm} = \pm\sqrt{2} \times \sqrt{h_0^2[1 + \cos(4kx_j - 2\phi)] + h_r^2[1 + \cos(2kx_j)]}$ .

In the limit  $h_r \rightarrow 0$  the two eigenvalues as a function of  $kx_j$  will cross at  $kx_j = \phi/2 + \pi/4$ . We can also find that when  $k_1x_j = \phi/2$  (for state  $|a\rangle$ ) and  $k_2x_j = \phi/2 + \pi/2$  (for state  $|b\rangle$ ), the eigenenergies are local minimal. The current

$\bar{J}_{AA} = \frac{2h_0}{N_{\text{lat}}} \sum_j \sin(\phi - 2kx_j)n_j^{(a)}$  and  $\bar{J}_{BB} = -\frac{2h_0}{N_{\text{lat}}} \sum_j \sin(\phi - 2kx_j)n_j^{(b)}$  are zero in this limit.

Now focusing on the case  $\phi = \pi/4$  and turning on the coupling  $h_r$  between the two states, the two local minimal points are coupled. When  $h_r \ll h_0$ , the two local minimal points are still nearly degenerate. The minimal points are shifted slightly with respect to  $k_1$  and  $k_2$ . We can expand the lower branch  $E_-$  of the eigenenergy around  $h_r \sim 0$  up to second order and find the shifts,  $\Delta k_1 x_j \approx -h_r^2 \sin \phi / 4h_0^2$  and  $\Delta k_2 x_j \approx -h_r^2 \sin \phi / 4h_0^2$ . The current  $\bar{J}_{AA} \approx \frac{2h_0}{N_{\text{lat}}} \sum_j \sin(-\Delta k_1)n_j^{(a)} \approx \frac{2h_0}{N_{\text{lat}}} \sum_j |\Delta k_1|n_j^{(a)} > 0$ . Similarly, we find that  $\bar{J}_{BB} > 0$ . Here  $\bar{J}_{AA} > \bar{J}_{BB}$  because the state  $|b\rangle$  is weakly occupied in the ground state, due to small  $h_r$ . This explains the results shown in the main text.

## EFFECTIVE DECAY RATE IN THE TRANSPORT OF SPIN WAVE STATES

We study the transportation of spin wave states by considering only the A-leg. The dynamics is governed by a master equation

$$\dot{\rho}_A = -i[H_A, \rho_A] + \sum_j \Gamma_j a_j \rho_A a_j^\dagger + 1/2\{a_j^\dagger a_j, \rho_A\}, \quad (\text{S20})$$

where the Hamiltonian reads  $H_A = -\sum_i (h_0 e^{i\phi} a_i^\dagger a_{i+1} + \text{H.c.})$ .

Decay rates of the central sites (index  $j = 0, 1$ ) are large and can be neglected at other sites, i.e.  $\Gamma_j > 0$  for  $j = 0, 1$  and  $\Gamma_j = 0$  otherwise. Far away from the center, the excitation propagates along the leg according to Hamiltonian  $H_A$ . Once approaching the middle sites, significant excitation loss takes place, when it hops from the nondecay neighboring site to the middle two sites. For situations shown in the main text, the hopping is from site  $j = 1$  to  $j = 0$ .

However the hopping is suppressed when the decay rate  $\Gamma_0$  is strong. To illustrate this, we consider the simplest model which contains only the two sites with index  $j = -1$  and  $j = 0$ . The initial state is  $|\psi(0)\rangle = |n_{-1}, n_0\rangle$  with  $n_{-1} = 1$  and  $n_0 = 0$  (the subscript indicates the site index.). This state couples to the state  $|\phi\rangle = |0, 1\rangle$ , which will decay at a rate  $\Gamma_0^{(0)}$ . The effective decay rate can be estimated through analyzing the non-Hermitian Hamiltonian [S74],  $H_e = H_c + H_d = (h_0 e^{i\phi} a_{-1} a_0^\dagger + \text{H.c.}) - i\Gamma_0/2 a_0^\dagger a_0$ , where the coupling  $H_c = (h_0 e^{i\phi} a_{-1} a_0^\dagger + \text{H.c.})$  and diagonal Hamiltonian  $H_d = -i\Gamma_0/2 a_0^\dagger a_0$ . The energy of the initial state in the presence of the coupling can be solved through the second order perturbation [S74]

$$E_0^{(2)} = \frac{\langle \psi(0) | H_c | \phi \rangle \langle \phi | H_c | \psi(0) \rangle}{-H_d} = \frac{h_0^2}{i\Gamma_0/2} = -\frac{2ih_0^2}{\Gamma}. \quad (\text{S21})$$

The initial state evolves according to  $|\psi(t)\rangle = \exp(-iE_0^{(2)}t)|\psi(0)\rangle$ . Hence the remaining probability of the initial state is

$$P = \langle \psi(t) | \psi(t) \rangle = \exp\left(-\frac{4h_0^2 t}{\Gamma_0}\right). \quad (\text{S22})$$

The initial state decays at an effective rate  $\Gamma_{\text{eff}} = 4h_0^2/\Gamma_0$ , which decreases with increasing  $\Gamma_0$ . Such an dependence is seen from the numerical calculations in the main text.

## EXPERIMENTAL PROPOSAL FOR REALIZING STRONGLY CORRELATED PHENOMENA

Chiral edge states can be realized in momentum space, either using mechanical momentum states of cold atoms [S78–S82], or collective excitation formed by collective excitations of electronic states [S83]. A unique advantage of the latter is that thermal resistant edge states can be probed, since the momentum-space lattice [S49, S75] of collective atomic excitations is immune to the motional entropy of atoms. The first proof-of-principle experiment has demonstrated chiral edge currents at the *room temperature* recently [S50]. However, electronic excited states suffer from fast spontaneous decay, inducing a steady state in the pump-dissipative system and destroying the *quantum* nature of the system. A clean *quantum* system in the momentum-space lattice in the presence of strong interactions is required to simulate strongly correlated phenomena.

### Realization for the Hamiltonian (1) without dissipation

We can get rid of the radiative dissipation by selecting three hyperfine spin states in ground levels of  $^{87}\text{Rb}$  with  $|g\rangle$  being  $|5^2S_{1/2}, F=1, m=1\rangle$ ,  $|a\rangle$  being  $|5^2S_{1/2}, F=1, m=-1\rangle$ , and  $|b\rangle$  being  $|5^2S_{1/2}, F=2, m=-2\rangle$ . The atomic level scheme and the configuration of the coupling beams are plotted in Fig. S3(a)(b). The spin states are split by a bias magnetic field. The inter-leg coupling  $h_r$  in purple is realized by Raman interaction which composed by the two fields around D1 line (in purple), while the one in blue is realized by a 6.8GHz microwave field. Since microwave field transfers negligible momentum, the MSL is slightly tilted in momentum space, as shown in Fig. S3(c). The intra-leg coupling  $h_0$  is implemented by the standing waves around D2 line, whose frequency is set in the middle point between  $a$  and  $b$  levels to introduce the  $\pi$  phase shift between the intra-leg couplings of A- and B-legs. The phase  $\phi$  in Ham. (1) can be controlled by manipulating the phase of the microwave and optical driving fields. Note here that, the small difference between the wave vectors of the standing wave is negligible. In the low-excitation regime, these atomic spin wave states are described by bosons [S84].

Here we choose Rydberg  $60S$  state as an example, whose lifetime is  $102 \mu\text{s}$ . With the detuning  $\Delta_d = 8 \text{ MHz}$  and Rabi frequency  $\Omega_R = 3 \text{ MHz}$  of the dressing laser, the effective lifetime in the Rydberg dressed state is  $2.9 \text{ ms}$ . We obtain  $r_c = 4.54 \mu\text{m}$  and  $V = 158.2 \text{ kHz}$ . This large soft-core radius  $r_c$  leads to a short-range interaction in momentum space, as it is far larger than the wavelength of the standing wave laser ( $\sim 780 \text{ nm}$ ). The inter- and intra-leg coupling strengths  $h_r$  and  $h_o$  can vary in a large parameter regimes. For example, we choose the parameters  $\Delta_{zeeman} = 50 \text{ MHz}$  being the Zeeman splitting between  $|g\rangle$  and  $|a\rangle$ ,  $\Delta_r = \Delta_a = \Delta_b = 3.4 \text{ GHz}$  being the detunings [see details in Fig. S3(a)],  $\Omega_s = 40 \text{ MHz}$  being the Rabi frequencies of optical fields with  $s = 0, 1, 2$ , and  $\Omega_{mw} = 500 \text{ kHz}$  being the effective Rabi frequency of the microwave field. The corresponding  $h_r$  and  $h_0$  are  $\sim 50 \text{ kHz}$  ( $\gg E_r \approx 4 \text{ kHz}$ , with  $E_r$  being the recoil energy), which are larger enough to observe coherent dynamics in microsecond timescale.

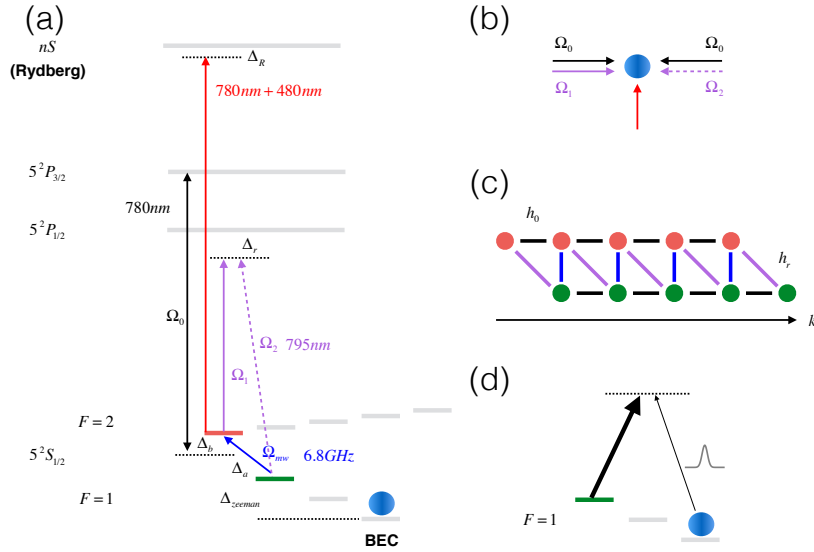


FIG. S3. (Color online) **Experimental setup.** (a) The atomic level scheme. (b) The configuration of the coupling optical fields. (c) The momentum space lattice. (d) The Raman coupling to prepare the initial state.

### Loading the excitations and measurement

To observe the dynamics in MSL, we need to initialize excitations in the A-leg with a post-selection process. The BEC is prepared in ground state before turning on the Ham. (1). Then we apply a strong classical field (thick) and a single photon (thin) in Fig. S3(d), forming a Raman coupling. When the single photon is not observed by a detector on its incident direction, we know one excitation is loaded in level  $a$  [S83]. Since the coherent time of level  $a$  is long enough, we can repeat the process twice to prepare the two-excitation state in zeroth site in A-leg. For the Zeno dynamics, we need to prepare a single excitation on the  $n$ th site in A-leg and introduce an effective decay to the zeroth one (see more details in the next subsection). After the single excitation is loaded into the zeroth site, we can

apply two  $\pi$ -pulses of blue and purple  $h_r$  couplings in a sequence. Such a pulse pair transport the excitation from the zeroth site to the first site in the A-leg. We can repeat the process for  $n$  times to finish the initialization.[S85].

We can also pump the excitation to the MSL when the Hamiltonian is on. By tuning the frequency of the pumping microwave field to the energy of the ground state in MSL, we can excite a specific state with high fidelity since the state width is very narrow. To prepare the total excitations  $N_{\text{tot}} \ll N_{\text{BEC}}$ , the pulse area of the pumping microwave field is roughly estimated as  $\sqrt{N_{\text{BEC}}}\Omega_p t = \pi N_{\text{tot}}$ , where  $\Omega_p$  is the effective Rabi frequency of the pumping microwave field,  $\sqrt{N_{\text{BEC}}}$  is the collective enhancement of  $N_{\text{BEC}}$  atoms, and  $t$  is the pulse duration.

By measuring the probability distribution of the  $a$ - and  $b$ -level atoms in momentum space via time of flight imaging, we can obtain the distribution of the excitation in MSL, which is expected to show the strongly correlated phenomena, *e.g.* ground state chiral current [S18], excitation blockade, and Zeno dynamics.

### Effective decay

In order to simulate the Zeno dynamics, we can replace the long-lived hyperfine states with low-lying decay states, realizing a superradiance lattice [S49], or incorporate an effective decay in the present setup. It could be realized by coupling the level  $a$  with a strong classical field off-resonantly. Spontaneous Raman process happens in a rare probability, which depends on the detuning. It's a reversal process of the state initialization as we mentioned above. The effective decay in zeroth site off A-leg is larger than the ones in other sites with a  $\sqrt{N_{\text{BEC}}}$  enhancement. In this way, we obtain a controllable decay term only in zeroth site when the atomic number is large enough.

- 
- [1] K. V. Klitzing, G. Dorda, and M. Pepper, *Physical Review Letters* **45**, 494 (1980).
- [2] D. J. Thouless, M. Kohmoto, M. P. Nightingale, and M. den Nijs, *Phys. Rev. Lett.* **49**, 405 (1982).
- [3] M. Z. Hasan and C. L. Kane, *Reviews of Modern Physics* **82**, 3045 (2010).
- [4] T. Senthil, *Annual Review of Condensed Matter Physics* **6**, 299 (2015).
- [5] J. Sinova, S. O. Valenzuela, J. Wunderlich, C. H. Back, and T. Jungwirth, *Reviews of Modern Physics* **87**, 1213 (2015).
- [6] T. H. Hansson, M. Hermanns, S. H. Simon, and S. F. Viefers, *Reviews of Modern Physics* **89**, 025005 (2017).
- [7] I. Bloch, J. Dalibard, and W. Zwerger, *Rev. Mod. Phys.* **80**, 885 (2008).
- [8] M. Lewenstein, A. Sanpera, and V. Ahufinger, *Ultracold Atoms in Optical Lattices: Simulating quantum many-body systems* (Oxford University Press, 2012).
- [9] S. L. Bromley, S. Kolkowitz, T. Bothwell, D. Kedar, A. Safavi-Naini, M. L. Wall, C. Salomon, A. M. Rey, and J. Ye, *Nature Physics* **14**, 399 (2018).
- [10] N. Goldman, J. C. Budich, and P. Zoller, *Nature Physics* **12**, 639 (2016).
- [11] J. Dalibard, F. Gerbier, G. Juzeliūnas, and P. Öhberg, *Rev. Mod. Phys.* **83**, 1523 (2011).
- [12] N. Goldman, G. Juzeliūnas, P. Öhberg, and I. B. Spielman, *Reports on Progress in Physics* **77**, 126401 (2014).
- [13] N. R. Cooper, J. Dalibard, and I. B. Spielman, *Rev. Mod. Phys.* **91**, 015005 (2019).
- [14] Y.-J. Lin, R. L. Compton, K. Jiménez-García, J. V. Porto, and I. B. Spielman, *Nature* **462**, 628 (2009).
- [15] Y. Lin, R. L. Compton, K. Jiménez-García, W. D. Phillips, J. V. Porto, and I. B. Spielman, *Nature Physics* **7**, 531 (2010).
- [16] M. Mancini, G. Pagano, G. Cappellini, L. Livi, M. Rider, J. Catani, C. Sias, P. Zoller, M. Inguscio, and M. Dal-
- 
- monte, *Science* **349**, 1510 (2015).
- [17] L. F. Livi, G. Cappellini, M. Diem, L. Franchi, C. Clivati, M. Frittelli, F. Levi, D. Calonico, J. Catani, M. Inguscio, and L. Fallani, *Phys. Rev. Lett.* **117**, 220401 (2016).
- [18] M. Atala, M. Aidelsburger, M. Lohse, J. Barreiro, B. Paredes, and I. Bloch, *Nature Physics* **10**, 588 (2014).
- [19] B. K. Stuhl, H.-I. Lu, L. M. Ayccock, D. Genkina, and I. B. Spielman, *Science* **349**, 1514 (2015).
- [20] J. H. Kang, J. H. Han, and Y. Shin, *Phys. Rev. Lett.* **121**, 150403 (2018).
- [21] M. Aidelsburger, M. Atala, S. Nascimbène, S. Trotzky, Y.-A. Chen, and I. Bloch, *Physical Review Letters* **107**, 487 (2011).
- [22] J. Struck, C. Ölschläger, M. Weinberg, P. Hauke, J. Simonet, A. Eckardt, M. Lewenstein, K. Sengstock, and P. Windpassinger, *Phys. Rev. Lett.* **108**, 225304 (2012).
- [23] M. Aidelsburger, M. Atala, M. Lohse, J. T. Barreiro, B. Paredes, and I. Bloch, *Phys. Rev. Lett.* **111**, 185301 (2013).
- [24] M. Hirokazu, G. A. Siviloglou, C. J. Kennedy, B. William Cody, and K. Wolfgang, *Physical Review Letters* **111**, 185302 (2013).
- [25] J. Gregor, M. Michael, D. Rémi, L. Martin, U. Thomas, G. Daniel, and E. Tilman, *Nature* **515**, 237 (2014).
- [26] C. J. Kennedy, W. C. Burton, W. C. Chung, and W. Ketterle, *Nature Physics* **11**, 1106 (2015).
- [27] N. Fläschner, B. S. Rem, M. Tarnowski, D. Vogel, D.-S. Lühmann, K. Sengstock, and C. Weitenberg, *Science* **352**, 1091 (2016).
- [28] L. Asteria, D. T. Tran, T. Ozawa, M. Tarnowski, B. S. Rem, N. Fläschner, K. Sengstock, B. Goldman, and C. Weitenberg, *Nature Physics* **15**, 449 (2019).
- [29] M. L. Wall, A. P. Koller, S. Li, X. Zhang, N. R. Cooper, J. Ye, and A. M. Rey, *Physical Review Letters* **116**, 035301 (2016).
- [30] X. Zhou, J.-S. Pan, Z.-X. Liu, W. Zhang, W. Yi, G. Chen, and S. Jia, *Phys. Rev. Lett.* **119**, 185701 (2017).
- [31] S. Kolkowitz, S. L. Bromley, T. Bothwell, M. L. Wall, G. E. Marti, A. P. Koller, X. Zhang, A. M. Rey, and

- J. Ye, *Nature* **542**, 66 (2016).
- [32] M. E. Tai, A. Lukin, M. Rispoli, R. Schittko, T. Menke, B. Dan, P. M. Preiss, F. Grusdt, A. M. Kaufman, and M. Greiner, *Nature* **546**, 519 (2017).
- [33] P. He, M. A. Perlin, S. R. Muleady, R. J. Lewis-Swan, R. B. Hutson, J. Ye, and A. M. Rey, 1904.07866 (2019).
- [34] H. Levine, A. Keesling, A. Omran, H. Bernien, S. Schwartz, A. S. Zibrov, M. Endres, M. Greiner, V. Vuletić, and M. D. Lukin, *Phys. Rev. Lett.* **121**, 123603 (2018).
- [35] A. Omran, H. Levine, A. Keesling, G. Semeghini, T. T. Wang, S. Ebadi, H. Bernien, A. S. Zibrov, H. Pichler, S. Choi, *et al.*, *Science* **365**, 570 (2019).
- [36] R. B. Laughlin, *Phys. Rev. Lett.* **50**, 1395 (1983).
- [37] S. de Léséleuc, V. Lienhard, P. Scholl, D. Barredo, S. Weber, N. Lang, H. P. Büchler, T. Lahaye, and A. Browaeys, *Science* **365**, 775 (2019).
- [38] A. Celi, B. Vermersch, O. Viyuela, H. Pichler, M. D. Lukin, and P. Zoller, arXiv preprint arXiv:1907.03311 (2019).
- [39] M. Saffman, T. G. Walker, and K. Mølmer, *Rev. Mod. Phys.* **82**, 2313 (2010).
- [40] I. Bouchoule and K. Mølmer, *Phys. Rev. A* **65**, 041803 (2002).
- [41] G. Pupillo, A. Micheli, M. Boninsegni, I. Lesanovsky, and P. Zoller, *Phys. Rev. Lett.* **104**, 223002 (2010).
- [42] N. Henkel, R. Nath, and T. Pohl, *Phys. Rev. Lett.* **104**, 195302 (2010).
- [43] J. Honer, H. Weimer, T. Pfau, and H. P. Büchler, *Phys. Rev. Lett.* **105**, 160404 (2010).
- [44] F. Cinti, P. Jain, M. Boninsegni, A. Micheli, P. Zoller, and G. Pupillo, *Phys. Rev. Lett.* **105**, 135301 (2010).
- [45] W. Li, L. Hamadeh, and I. Lesanovsky, *Phys. Rev. A* **85**, 053615 (2012).
- [46] A. D. Bounds, N. C. Jackson, R. K. Hanley, R. Faoro, E. M. Bridge, P. Huillery, and M. P. A. Jones, *Phys. Rev. Lett.* **120**, 183401 (2018).
- [47] Y.-Y. Jau, A. M. Hankin, T. Keating, I. H. Deutsch, and G. W. Biedermann, *Nature Physics* **12**, 71 (2016).
- [48] J. Zeiher, R. Van Bijnen, P. Schauß, S. Hild, J.-y. Choi, T. Pohl, I. Bloch, and C. Gross, *Nature Physics* **12**, 1095 (2016).
- [49] D.-W. Wang, R.-B. Liu, S.-Y. Zhu, and M. O. Scully, *Phys. Rev. Lett.* **114**, 043602 (2015).
- [50] H. Cai, J. Liu, J. Wu, Y. He, S.-Y. Zhu, J.-X. Zhang, and D.-W. Wang, *Phys. Rev. Lett.* **122**, 023601 (2019).
- [51] I. Vasić, A. Petrescu, K. Le Hur, and W. Hofstetter, *Phys. Rev. B* **91**, 094502 (2015).
- [52] K. Plekhanov, I. Vasić, A. Petrescu, R. Nirwan, G. Roux, W. Hofstetter, and K. Le Hur, *Phys. Rev. Lett.* **120**, 157201 (2018).
- [53] E. Orignac and T. Giamarchi, *Phys. Rev. B* **64**, 144515 (2001).
- [54] O. Boada, A. Celi, J. I. Latorre, and M. Lewenstein, *Phys. Rev. Lett.* **108**, 133001 (2012).
- [55] A. Petrescu and K. Le Hur, *Phys. Rev. Lett.* **111**, 150601 (2013).
- [56] A. Celi, P. Massignan, J. Ruseckas, N. Goldman, I. B. Spielman, G. Juzeliūnas, and M. Lewenstein, *Phys. Rev. Lett.* **112**, 043001 (2014).
- [57] E. Anisimovas, M. Račiūnas, C. Sträter, A. Eckardt, I. B. Spielman, and G. Juzeliūnas, *Phys. Rev. A* **94**, 063632 (2016).
- [58] M. Calvanese Strinati, E. Cornfeld, D. Rossini, S. Barbarino, M. Dalmonte, R. Fazio, E. Sela, and L. Mazza, *Phys. Rev. X* **7**, 021033 (2017).
- [59] H. M. Price, T. Ozawa, and N. Goldman, *Phys. Rev. A* **95**, 023607 (2017).
- [60] B. Sundar, B. Gadway, and K. R. Hazzard, *Scientific reports* **8**, 3422 (2018).
- [61] S. N. L. Barbiero, L. Chomaz and N. Goldman, arXiv preprint arXiv:1907.10555 (2019).
- [62] F. London, *J. Phys. Radium* **8**, 347 (1937).
- [63] N. Byers and C. N. Yang, *Phys. Rev. Lett.* **7**, 46 (1961).
- [64] F. Bloch, *Phys. Rev.* **137**, A787 (1965).
- [65] Y. I. M. Buttiker and R. Landauer, *Phys. Lett. A* **96**, 365 (1983).
- [66] A. C. Bleszynski-Jayich, W. E. Shanks, B. Peaudecerf, E. Ginossar, F. von Oppen, L. Glazman, and H. J. G. E, *Science* **326**, 272 (2009).
- [67] We consider the system with lattice sites up to  $N_{\text{lat}} = 256$  to verify the finite-size effects on phase diagrams.
- [68] Y.-Q. Li, M. R. Bakhtiari, L. He, and W. Hofstetter, *Phys. Rev. B* **84**, 144411 (2011).
- [69] B. Capogrosso-Sansone, N. V. Prokof'ev, and B. V. Svistunov, *Phys. Rev. B* **75**, 134302 (2007).
- [70] E. Urban, T. A. Johnson, T. Henage, L. Isenhower, D. D. Yavuz, T. G. Walker, and M. Saffman, *Nat. Phys.* **5**, 110 (2009).
- [71] A. Gaetan, Y. Miroshnychenko, T. Wilk, A. Chotia, M. Viteau, D. Comparat, P. Pillet, A. Browaeys, and P. Grangier, *Nat. Phys.* **5**, 115 (2009).
- [72] A. Svidzinsky and J.-T. Chang, *Phys. Rev. A* **77**, 043833 (2008).
- [73] M. O. Scully and M. S. Zubairy, *Quantum Optics*, 1st ed. (Cambridge University Press, 1997).
- [74] A. J. Daley, arXiv:1405.6694 [cond-mat, physics:quant-ph] (2014).
- [75] L. Chen, P. Wang, Z. Meng, L. Huang, H. Cai, D.-W. Wang, S.-Y. Zhu, and J. Zhang, *Phys. Rev. Lett.* **120**, 193601 (2018).
- [76] A. Georges, G. Kotliar, W. Krauth, and M. J. Rozenberg, *Rev. Mod. Phys.* **68**, 13 (1996).
- [77] K. Byczuk and D. Vollhardt, *Phys. Rev. B* **77**, 235106 (2008).
- [78] B. Gadway, *Phys. Rev. A* **92**, 043606 (2015).
- [79] F. A. An, E. J. Meier, and B. Gadway, *Science advances* **3**, e1602685 (2017).
- [80] F. A. An, E. J. Meier, J. Ang'ong'a, and B. Gadway, *Phys. Rev. Lett.* **120**, 040407 (2018).
- [81] F. A. An, E. J. Meier, and B. Gadway, *Phys. Rev. X* **8**, 031045 (2018).
- [82] E. J. Meier, F. A. An, A. Dauphin, M. Maffei, P. Massignan, T. L. Hughes, and B. Gadway, *Science* **362**, 929 (2018).
- [83] M. O. Scully, E. S. Fry, C. H. R. Ooi, and K. Wódkiewicz, *Phys. Rev. Lett.* **96**, 010501 (2006).
- [84] M. Fleischhauer and M. D. Lukin, *Phys. Rev. Lett.* **84**, 5094 (2000).
- [85] D.-W. Wang and M. O. Scully, *Physical Review Letters* **113**, 083601 (2014).